



Universiteit
Leiden
The Netherlands

Mitochondria in chemical-induced toxicity

Stel, W. van der

Citation

Stel, W. van der. (2022, February 1). *Mitochondria in chemical-induced toxicity*. Retrieved from <https://hdl.handle.net/1887/3270836>

Version: Publisher's Version

License: [Licence agreement concerning inclusion of doctoral thesis in the Institutional Repository of the University of Leiden](#)

Downloaded from: <https://hdl.handle.net/1887/3270836>

Note: To cite this publication please use the final published version (if applicable).



**Mitochondrial
fragmentation through
OPA1-cleavage in
response to ETC inhibition
is driven by a combination
of reduced ATP and
increased MMP**

Wanda van der Stel, Huan Yang, Sylvia le Dévédec, Bob van de Water,
Joost Beltman, Erik H.J Danen[#]

Submitted to Cell. Bio. Toxicol

Cells can adjust their mitochondrial morphology by altering the balance between mitochondrial fission and fusion to adapt to stressful conditions. Mitochondria can fuse together upon energy shortage, to enlarge their ATP producing capacity, or they can fragment, to facilitate mitochondrial transport or mitophagy. Such phenotypical alterations could serve as a biomarker for the changes in the underlying mitochondrial processes in the context of chemical-induced toxicity. However, the connection between a chemical perturbation, changes in mitochondrial function, and altered mitochondrial morphology is not well understood. Here, we systematically assessed the effects of distinct classes of electron transport chain (ETC) perturbing agents on mitochondrial membrane potential (MMP), ATP production, mitochondrial morphology, and cell viability using a combination of experimental and computational approaches. Mitochondrial morphology phenotypes were clustered based on high content confocal imaging data and machine learning algorithms and mitochondrial integrity patterns were mapped including temporal and spatial resolutions. Changes in MMP and viability were assessed by imaging and mitochondrial and cellular ATP levels were measured biochemically and using FRET biosensors, and the role of OPA1 post-translational modification as a mechanism connecting functional and morphological adaptation in mitochondria was explored. Our results show that inhibition of mitochondrial ATP production and oxygen consumption rate is insufficient to trigger OPA1 cleavage and mitochondrial fragmentation, whereas the combination of ATP reduction and increase of MMP did provoke a change in mitochondrial morphology. Altogether, our findings connect vital mitochondrial functions and mitochondrial phenotypes that help understanding of cellular toxicity caused by ETC perturbing chemicals.

Keywords: mitochondria, morphology, machine learning, membrane potential, ATP

Introduction

Mitochondrial malfunctioning plays a role in chemical induced toxicities and various diseases [Pacheu-Grau 2018, Dykens 2007]. Disease-related mitochondrial defects e.g., associated with Parkinson and Alzheimer disease, can be frequently traced back to mutations in genes involved in the major functions of the mitochondria [De Castro 2010, Pacheu-Grau 2018]. Chemical-induced mitochondrial stress stimulates the cell to rearrange its mitochondrial pool and induce adaptive signaling responses in order to cope with reduced cellular functioning [Han 2013]. An inability to recover from the mitochondrial insult, will induce apoptosis and/or necrosis to sacrifice the injured cell. Prolonged stress causing excessive cell death, will result in organ failure [Bock 2009]. Unraveling the concentration- and time-resolved relationships between mitochondrial perturbation and toxicity will provide useful information for chemical safety prediction and provide insight in adaptive and toxic responses to mitochondrial stress.

The type of chemical-insult dictates the type of cellular-mitochondrial responses. Chemicals may directly target key mitochondrial proteins such as electron transport chain (ETC) components or cause cellular stress leading indirectly to damaged mitochondria. In response, mitochondria can trigger a mitochondrial unfolded protein response (UPR_{mt}) to refold incorrectly assembled proteins [Münch 2018, Qureshi 2017], activate mitochondrial biogenesis to increase size and numbers of mitochondria [Jornayvaz 2010, Hock 2009], adapt mitochondrial morphology and remodel ETC to increase oxidative phosphorylation (OXPHOS) capacity [Westermann 2010, Youle 2012], and initiate mitophagy to dispose of malfunctioning mitochondria [Youle 2011, Hamacher-Brady 2016]. The specificity of these mitochondrial responses for certain types of stress could be used to understand and predict the type of chemical-induced perturbation.

Among the mitochondrial responses, morphological remodeling is one of the fastest and most flexible adaptation programs. Even under healthy conditions mitochondria are highly dynamic organelles that constantly adapt their appearance based on the energy demand in various regions of the cells and facilitate mitophagy to get rid of undesired mitochondria [Westermann 2010, Giacomello 2020]. Different mitochondrial morphologies have been recorded in cell lines upon mitochondrial toxicant exposure, including antimycin, FCCP, oligomycin and rotenone [Leonard 2015, Koopman 2005, Koopman 2006, Miyazono 2018]. These morphologies have been classified as puncta, rods, networks, small/large, etc. The presence of larger mitochondrial networks facilitates energy production, because of the increased interconnected membrane surfaces which can support OXPHOS. The formation of smaller mitochondria increases their mobility supporting energy demand in the outer areas of the cells, but also simplifies degradation when desired [Westermann 2010].

Increasing and decreasing mitochondrial surface is achieved by changing the balance between fission and fusion [Seo 2010]. The machinery responsible for fission and fusion consists of a core group of GTPases: DRP1 is mostly responsible for fission and MFN1, MFN2 and OPA1 are responsible for fusion [Westermann 2010]. Fission is achieved by dephosphorylation and polymerization of DRP1 at ER-mitochondrial sites. Fusion of mitochondria is initiated by the outer membrane protein MFN, which connects the outer membranes of two mitochondria and is subsequently followed by fusion of the inner membranes, which is facilitated by OPA1 [Giacomello 2020]. The exact trigger for the activation of the various fission and fusion related GTPases is not completely understood. Some of the GTPase members are activated via post-translational modification including cleavage and phosphorylation [Cribbs 2007, Jahani-Asl 2007, MacVicar 2016]. Under healthy conditions, OPA1 is imported into the mitochondria and cleaved by the mitochondrial processing peptidase (MPP) into a long transmembrane protein (long OPA1/ L-OPA1) which supports the fusion process. Stress may activate two proteases, OMA1 and YME1L, that cleave OPA1 resulting in a shorter non-membrane bound form (short OPA1/ S-OPA1), which does not support fusion. Reported triggers that stimulate OPA1 cleavage and inhibit fusion include decreased ATP levels, a drop in mitochondrial membrane potential (MMP), heat shock, and the loss of mitochondrial DNA [Anand 2014, Baker 2014, Ehses 2009, Head 2009, Consolato 2018].

Here, we addressed whether changes in mitochondrial morphology can be coupled to key aspects of mitochondrial function in the context of chemical-induced toxicities. For this purpose, we systematically assessed the effect of distinct classes of ETC perturbing agents in a time- and concentration-resolved manner. We established high-content imaging methods and computational modeling to categorize mitochondrial morphology and monitor changes in ATP levels and MMP dynamics. This data was combined with an analysis of proteolytic cleavage of OPA1 as a key step in mitochondrial fusion. Lastly, we used gene silencing to address the impact of interfering with morphological adaptation on adaptation to mitochondrial stress. Our findings shed light on the dynamic relation between mitochondrial morphology and function in the context of chemical-induced stress and create the opportunity to use mitochondrial morphology changes as a biomarker for the underlying mitochondrial perturbation.

Materials and Methods

Chemicals

All tested chemicals were purchased via Sigma Aldrich (Germany): antimycin A (A8674), cyclosporin A (30024), DCCD (D80002), diafenthuron (31571), oligomycin (O4876), rotenone (R8875). The larger set of chemicals used to study difference between complex inhibitors was obtained via the JRC (Ispra Italy): capsaicin (Cat.

No. M2028), deguelin (D0817), fenpyroximate (31684), pyrimidifen (35999), rotenone (R8875), tebufenpyrad (46438), carboxin (45371), mepronil (33361), thifluzamide (49792), antimycin A (A8674), azoxystrobin (3167), cyazofamid (33874), picoxystrobin (33568), pyraclostrobin (33696). Stocks were created in dimethyl sulfoxide (DMSO) and stored at -80°C/-30°C until further usage. Exposure medium was created at the day of usage and contained a max of 0.2% (v/v) DMSO.

Cell culture

All experiments were performed using HepG2 cells purchased from ATCC (American Type Culture Collection, Wesel, Germany). Cells were maintained in complete medium at 37°C in a 5% CO₂ humidified atmosphere. The complete medium consisted of Dulbecco's modified Eagle's medium (DMEM) (Fisher Scientific, 11504496), supplemented with 10% (v/v) FBS (fetal bovine serum), 25 U/ml penicillin and 25 µg/mL streptomycin (FBS; South American, Fisher Scientific, S181L-500 & PenStrep, Fisher Scientific, 15070-063). For experiments that require inhibition of the glycolysis the medium was extra supplemented with 10mM 2-deoxyglycose (2DG) (Sigma-Aldrich, D8375-5G) at the moment of exposure.

Creation of HepG2 cell lines containing OPA-GFP or ATP-biosensors

OPA1 fused to GFP was introduced in HepG2 cells using the BAC technology previously optimized in our lab [Wink 2017, Poser 2008]. HepG2 cells containing ATP-biosensors located in the mitochondria or cytoplasm were created using constructs kindly provided by Hiromi Imamura (Precursory Research for Embryonic Science, Japan Science and Technology Agency) [Imamura 2009]. Both for the BAC-GFP and the ATP biosensors constructs, 8µg DNA was introduced using lipofectamine2000 (Fisher Scientific, 11668-027) into 2.000.000 HepG2 cells. Cells were kept on G418 (PAA/Brunschwig chemie, P31-011) selection starting with 0.25mg/ml until confluency followed by 0.5mg/ml until colony formation. Confocal imaging was used to quickly select for GFP positive colonies (both for the OPA1-GFP and the ATP biosensor cell lines). The used OPA1-GFP clone was selected based on protein size in western blot. The used ATP biosensor was selected based on a homogenous expression.

siRNA transfection

siRNAs targeting OPA1 (SMARTpool of 4 single siRNAs = MQ-005273-00-0002, siRNA1 = D-005273-01, siRNA2 = D-005273-02, siRNA3 = D-005273-03, siRNA4 = D-005273-04) were purchased from Dharmacon (US). Reverse transfections were performed in 24-wells plates (Costar, 3524) or 96-well screenstar black plate (Greiner Bio-One, 655892, 655866) using 40 or 50nM siRNA and the transfection reagent INTERFERin (Polyplus, 409-50) in a dilution of 1:1000 or 1:1250. siRNA were

diluted to 1 μ M in 1x siRNA buffer (Dharmacon, B-002000-UB-100). INTERFERin was diluted 50x in SFM and antibiotic free medium. Upon 5 minutes incubation at RT both solutions were mixed in a 1:3 (siRNA/INTERFERIN) ratio and incubated for 20-30min at RT. Cell mixtures of 476,191 cells/well (24-well) or 23,000 cells/well (96-well) in medium containing FBS and antibiotics were mixed in a ratio of 6.25:1 or 5:1 to the siRNA-INTERFERin mixture, respectively. 24h after transfection the medium was refreshed and 72h after transfection chemical exposure followed by the desired readout were performed. Mock and KP (a mixture of 720 siRNA SMARTpools originating from the siGENOME human protein kinase library) were used as controls.

Confocal live cell imaging and analysis of MMP

Effects of chemical exposure on MMP was assessed using Rhodamine123 (Rho123) (sigma Aldrich, R8004) using the protocol described previously [van der Stel 2020]. Cells were seeded two days before exposure. At the day of exposure cells were first co-stained with 200ng/ μ L Hoechst (Life technologies, H1399) and 1 μ M Rho123 for 75min, followed by a co-staining of 0.2 μ M Rho123 and 100nM propidium iodide (PI) (Sigma-Aldrich, P4170) and exposure to the desired concentration of test chemical. Over a period of 24h the signal intensity of Hoechst (408nm), rho123 (448nm) and PI (561nm) were monitored every hour. The nuclei were identified based the Hoechst picture and formed the basis for the assessment of the cytoplasm (n distance around nucleus). Finally, the intensity of the rho123 was assessed in the cytoplasm and the cell death based on the fraction of nuclei that showed co-staining of Hoechst and PI. Part of the MMP data were used for development of a dynamic model and integration with RNA-seq data elsewhere [van der Stel 2021].

Confocal live cell imaging and analysis of ATP-biosensor

Effects of chemical exposure upon ATP fluctuations in the cytoplasm and mitochondria of HepG2 cells were assessed using the stably integrated ATP-biosensor constructs. The experiments were performed as previously described [van der Stel 2020]. Cells were seeded two days before chemical exposure. Imaging was performed every 5minutes starting with two rounds of background measurement, followed by exposures and 2h of imaging. The sensor was excited with the 408nm laser and the FRET ratio was based on the emission at 408 and 488nm. The obtained 408nm images were used to determine the relevant cell area in which the 408 and 488 pixel intensities were determined. Part of the ATP data were integration with RNA-seq data elsewhere [van der Stel 2021].

Confocal live cell imaging of mitochondrial morphology

Mitochondrial morphology was monitored using MitoTracker Red CMXRos (cell signaling, 9082) in a live confocal imaging setting. HepG2 cells were seeded with a density of 22.000 cells/well in a 96-wells glass/screenstar black plate (Greiner Bio-One, 655892, 655866). Two days after seeding cells were stained for 60min at 37° C with 200 ng/mL Hoechst 33342 (Life technologies, H1399) and 0.05µM MitoTracker Red. After 60min the medium was replaced with complete DMEM containing 0.013µM MitoTracker Red plus the desired concentration test chemical. The Hoechst and MitoTracker Red signal (respectively 408 and 561nm) were monitored at the desired time points using in total 120x zoom (60x objective plus 2x digital zoom or 40x objective plus 3x zoom) in a Nikon TiE2000 with perfect Focus System and xy-stage (Nikon, Amsterdam, The Netherlands).

Imaging data analysis for mitochondrial morphology data

Nuclei segmentation: CellProfiler (version 2.1.1 Broad Institute, Cambridge, USA) was used for the identification of nuclear objects. An in-house implemented segmentation module [Di 2012] based on watershed algorithms designed for extra zoom pictures was used to segment nuclear object from Hoechst intensity pictures, which were first equalized using a Gaussian filter.

Mitochondrial segmentation and feature quantification: Ilastik version 1.3.2post2 with a pixel classification workflow was used to identify MitoTracker Red positive pixels from background pixels [Berg 2019, Sommer 2011]. The pixel classification workflow consists of: feature selection, training and classification. First, two filters were selected based on visual inspection: *Laplacian of Gaussian* ($\sigma = 3.5$) in 2D and *Difference of Gaussians* ($\sigma = 3.5$) in 2D. Secondly, fore and background were annotated based on manual inspection of representative MitoTracker Red pictures. Next, a Random Forest classifier is used to classify all pixels into fore and background based on the selected features and annotations. Finally, the output from the pipeline is a "Simple Segmentation" picture, a binary picture with only fore and background classification. Afterwards, a custom python scripts was developed to utilize the Ilastik template in a headless mode, resulting in segmented mitochondrial objects in binary images. Subsequently, four features were used to describe object size and shape: area, perimeter, formfactor and solidity. The area describes the size of the objects in a number of pixels. The perimeter is the number of pixels at the boundary of an object. In the case of object with a hole, the perimeter is the sum of both inner and outer circle (i.e. the total length of the boundary between object and background). The formfactor is defined as $(4 * \pi * Area) / Perimeter$. The solidity is the quantification of the extent to which a shape is convex or concave. It is defined as $Area / ConvexArea$

(ConvexArea = the area enclosed by a convex hull/minimal convex object which can enclose the object).

Fitting with a Gaussian mixture model: A Gaussian mixture model (GMM) was applied to classify the segmented mitochondria objects in an unsupervised manner based on the 4 object features. In this way, the objects were divided into two categories, referred to as “fragmented” or “fused”. The model was trained using all experimental images of cells exposed to various mitochondrial complex inhibitors and a vehicle control condition at time points ranging from 1h to 24h. The GMM was implemented in python using 100 random starting values for the Gaussians. For each starting value, an expectation–maximization algorithm was utilized to minimize the negative *–log likelihood* of the data. Finally, the model with the lowest negative *–log likelihood* was selected as the best fit. The class to which each mitochondrial object belonged was determined based on the probability for the two classes (i.e., class having the highest probability was selected).

Statistical test: To compare control, compound exposure, and siRNA treatment, the ANOVA test combined with a Dunnett test were applied to analyze statistical significance.

Implementation: All data analyses were implemented in Linux with python 2.7 with packages scikit-learn for the GMM fitting and prediction, dash for interactive plotting and scipy.stats for statistical testing.

ATPlite assay and analysis

ATP levels were assessed in cell lysate upon 2 and 24h chemical exposure as previously described [van der Stel 2020]. Cells were seeded two days before exposure. At the third day cells were stained with Hoechst for 2hours followed by chemical exposure. 1h before the end of the exposure period the cells were imaged to monitor the Hoechst intensity. The Hoechst intensity pictures were used to segment the nuclear objects in every picture and the total nuclear count per image was used to normalized further measurements. After the desired exposure period the medium was replaced by Hanks' buffer including 5 mM HEPES, 250 mM sucrose, 25 mM TRIS, 3 mM EGTA, 5 mM MgCl₂, 5 mM succinate and 5 mM glutamate (37 °C, pH 7.3) and for the mitochondrial fraction also supplemented for 30-45sec with 150µM digitonin. ATP content was determined using the ATPlite 1 step Luminescence Assay reagent kit (PerkinElmer, 6016731). ATP data were integration with RNA-seq data elsewhere [van der Stel 2021].

Western Blot

OPA1-GFP cleavage was monitored using western blot. Cells were plated at a density of 200,000 cells/well in 24wells (Corning, 3524). Two days after seeding the cells were exposed to the test chemical for the desired timespan and lysed using direct lysis in 1x times sample buffer (stock: 1% BromoPhenolBlue (Sigma, B0126-25G) in MQ plus few drops of NaOH to dissolve BPB) supplemented with 5% v/v β -mercaptoethanol (Fisher Scientific, 125472500). Samples were heat-denatured for 10min at 95°C before usage. Proteins were separated using SDS-PAGE on gels consisting of a running and stacking gel. The running contained per 10ml: 5mL MilliQ, 2.5mL Acrylamide (Bio-Rad, 1610158), 2.5mL Tris (1.5M Tris, with 10% SDS and pH = 8.8), 75 μ L 10% APS (Ammonium PerSulfate) (Sigma, A3678-25g) and 15 μ L TEMED (VWR, 17-1312-01). The stacking gel contained per 10mL: 6.1mL MilliQ, 1.3mL Acrylamide, 2.5mL Tris (0.5M Tris, with 10% SDS and pH = 6.8), 75 μ L 10% APS and 15 μ L TEMED. The proteins were blotted onto a PVDF membrane (Sigma, IPVH00010) using a wet transfer system. Membranes were incubated in 1% m/v milk in 1%TBS plus Tween20 (Boom, P2287-500mL). Primary and secondary antibodies were diluted in TBS-Tween20, respectively 1:1000 and 1:2000. The used primary antibodies were mouse-anti-GFP (11814460001, Roche) and mouse-anti-tubulin (T-9026, Sigma), detected respectively using goat-anti-mouse-HRP (115-035-003, Jackson) and goat-anti-mouse-Cy5 (115-605-146, Jackson). The horseradish peroxidase activity and Cy5 signal were detected using the Image Quant LAS4000 (GE HealthCare).

Resazurin assay

The resazurin assay was conducted as previously described (van der Stel 2020). Briefly, the supernatant was replaced, after the assessment of the mitochondrial membrane potential, with 44 μ M resazurin dissolved in cell culture medium and incubated for 1.5 h in 5% CO₂ at 37°C. The colorimetric change upon resazurin reduction was assessed using 540nm excitation and 590nm emission.

Results

Analysis pipeline for quantitative categorization of mitochondrial morphology

To assess the link between mitochondrial morphology and mitochondrial perturbation, we assembled an analysis pipeline to classify mitochondrial morphology into two morphology subclasses (“fragmented” and “fused”). To make this pipeline compatible with high throughput data collection and include an unbiased morphology classification, we selected an unsupervised machine learning approach combined with open analysis software (Ilastik and CellProfiler) to segment and assess mitochondrial

objects in living cells (HepG2) stained with MitoTracker Red and imaged using confocal microscopy (Fig. 1A).

Step one of the pipeline included identification of mitochondria from live confocal images in which mitochondria were stained with MitoTracker Red. Ilastik software was used to classify pixels of the MitoTracker Red images into fore- and background (Fig. 1B). In step two, CellProfiler was used to segment mitochondrial objects and quantify 4 features per object: area, perimeter, formfactor and solidity (Fig. 1C). The third step consisted of an unsupervised learning approach using a Gaussian mixture model (GMM) to subdivide segmented mitochondrial objects based on the assessed features into two groups, i.e. fragmented and fused.

The parameter probability prediction from the GMM includes a mean and variance parameter per selected mitochondrial feature for both fragmented and fused mitochondria [Reynolds, 2009] (Fig. 1D). To evaluate the effect of data size on GMM fitting, we monitored the effects on the mean and variance of the Gaussians when changing 3 aspects, i.e., the number of compounds, the number of images and the number of objects. The effect of compound choice was studied using a leave-one-out strategy. The influence of the number of images was tested using 100 randomly selected subsets of the images (each time consisting of half of the images). Similarly, the effect of object number was estimated using only a fraction of all objects pooled from all conditions (using the fraction 1/2, 1/10, and 1/500 of all objects). This analysis showed that the data is sufficient to provide robust parameter estimates for the two mitochondrial classes (Fig. 1D). Moreover, visualization of the four considered features in two-dimensional scatter plots along with their estimated Gaussians demonstrated an excellent fitting performance (Fig. 1E).

ETC inhibitors disconnect mitochondrial morphology, membrane potential, and ATP production

To be able to use mitochondrial morphology classification as a toxicity biomarker it is important to understand the relationship between the readout and the biological effect. Alterations of mitochondrial morphology have previously been linked to distinct key functional properties including ATP levels and MMP [Anand 2014, Baker 2014, Ehes 2009, Head 2009, Consolato 2018]. We examined this relationship in the context of 3 known mitochondrial complex inhibitors: Rotenone, Antimycin and Oligomycin, targeting ETC complex I, III, and V, respectively (Fig. 2A).

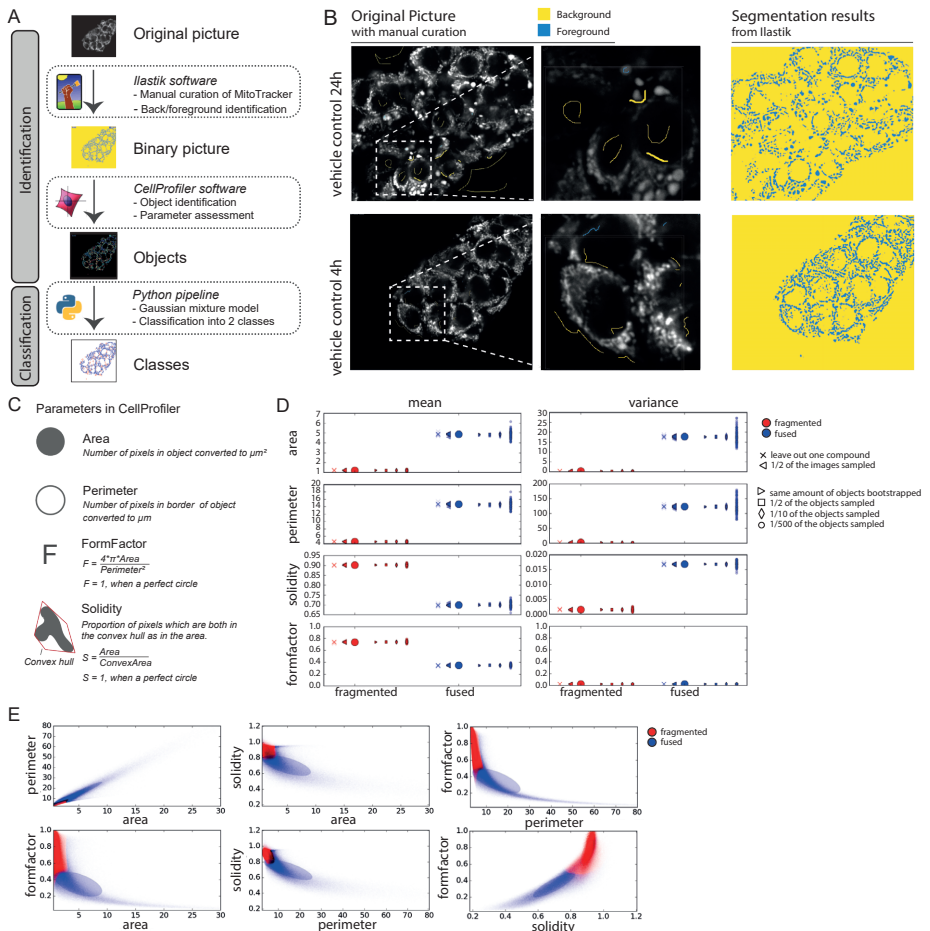


Figure 1: Quantification of mitochondrial morphology

A) schematic representation of the pipeline used to analyze mitochondrial morphology. The pipeline is designed to assess mitochondrial morphology in an unbiased approach using confocal images of mitochondria stained with MitoTracker Red in HepG2 cells. 1) The intensity pictures are converted to binary pictures using Ilastik software and based on manual curation, 2) Various features are collected of the identified objects using CellProfiler, 3) These features are used to classify all mitochondria into 2 classes using a machine learning approach. **B)** Manual curation of mitochondrial staining in the original MitoTracker Red images using Ilastik and the segmentation result from Ilastik based on the manual curation (yellow = background, blue = foreground). **C)** The selected parameters from CellProfiler software **D)** Effect of the data size on the estimated mean and variance for the four morphological features in the Gaussian mixture model. Red for fragmented mitochondria and blue for fused mitochondria **E)** Scatter plot of two features (area, perimeter, solidity, formfactor) to describe mitochondrial morphology for mixture of two subpopulations. Red for fragmented mitochondria and blue for fused mitochondria. The ellipse kernels represent the Gaussian distribution for the two subpopulations (red for fragmented and blue for fused population). Mean and co-variance info are utilized to draw those ellipses. The contour lines indicating 95% confidence interval of the parameters.

Exposure to a concentration range of oligomycin induced an increase in fragmented mitochondria (Fig. 2B, C). Rotenone treatment did not result in a shift in the identified mitochondrial populations. Antimycin exposure induced a slight decrease in fragmented mitochondria (i.e., an increase in fused mitochondria) at higher concentrations.

Morphological responses were compared to changes in MMP. Rotenone and antimycin each triggered a concentration dependent decrease in MMP (Fig. 2D; 1st column). By contrast, oligomycin stimulated a concentration-dependent increase of the MMP. The latter could be explained by blockage of ATP synthase, causing a proton gradient that is not used for ATP production [Symersky 2012, Hong 2008].

Additionally, morphological responses and MMP dynamics were compared to changes in ATP production. Rotenone, Antimycin and Oligomycin each caused a concentration-dependent drop in ATP levels in the cytoplasm as measured by a cytoplasmic ATP sensor (Fig. 2D; 2nd column; Suppl. fig 1A). Likewise, measurements using an ATP sensor localized to mitochondria showed that exposure to each of these chemicals resulted in a decrease in mitochondrial ATP and this drop was considerably faster than what was observed in the cytoplasmic compartment (Fig. 2D; 3rd column; Suppl. fig 1A). As an alternative approach ATP lite was used to measure overall whole cell ATP levels and ATP in the isolated mitochondrial fraction (Suppl. fig 1B). Both demonstrated a similar concentration-response relationship for Rotenone, Antimycin and Oligomycin as observed with the ATP-biosensors, with the mitochondrial ATP fraction almost completely disappearing upon chemical exposure, when compared to the negative control.

In conclusion, while the three distinct ETC inhibitors caused a similar decrease in mitochondrial ATP production, time and concentration-resolved analysis disconnected the responses at the level of mitochondrial morphology, MMP, and ATP production.

OPA1 cleavage links ETC inhibition to morphological adaptation

To address the role of known mitochondrial morphology regulators in the occurrence of the fragmentation phenotype, we silenced the *DRP1*, *OMA1* and *OPA1* genes and investigated the effect on mitochondrial morphology. Depletion of the fission protein DRP1 resulted as expected in a decrease in the number of fragmented mitochondria (Fig. 3A, B). OPA1 depletion caused an increase in mitochondrial fragmentation that was pronounced 96h after KD as was also observed with oligomycin. Depletion of the OPA1 regulator OMA1 did not result in a pronounced effect on mitochondria fragmentation. To further investigate the relationship between OPA1 and chemical-induced fragmentation, we developed an OPA1-GFP BAC fusion cell line (Fig. 3C) and used OPA1 silencing to validate the specific detection of long and short OPA1 by GFP antibody in this cell line (Fig. 3D; Suppl. fig 2A). The OPA1-GFP fusion protein localized in mitochondrial like structures in the cell and co-staining using a MitoTracker Red marker demonstrated overlap as expected (Fig. 3E).

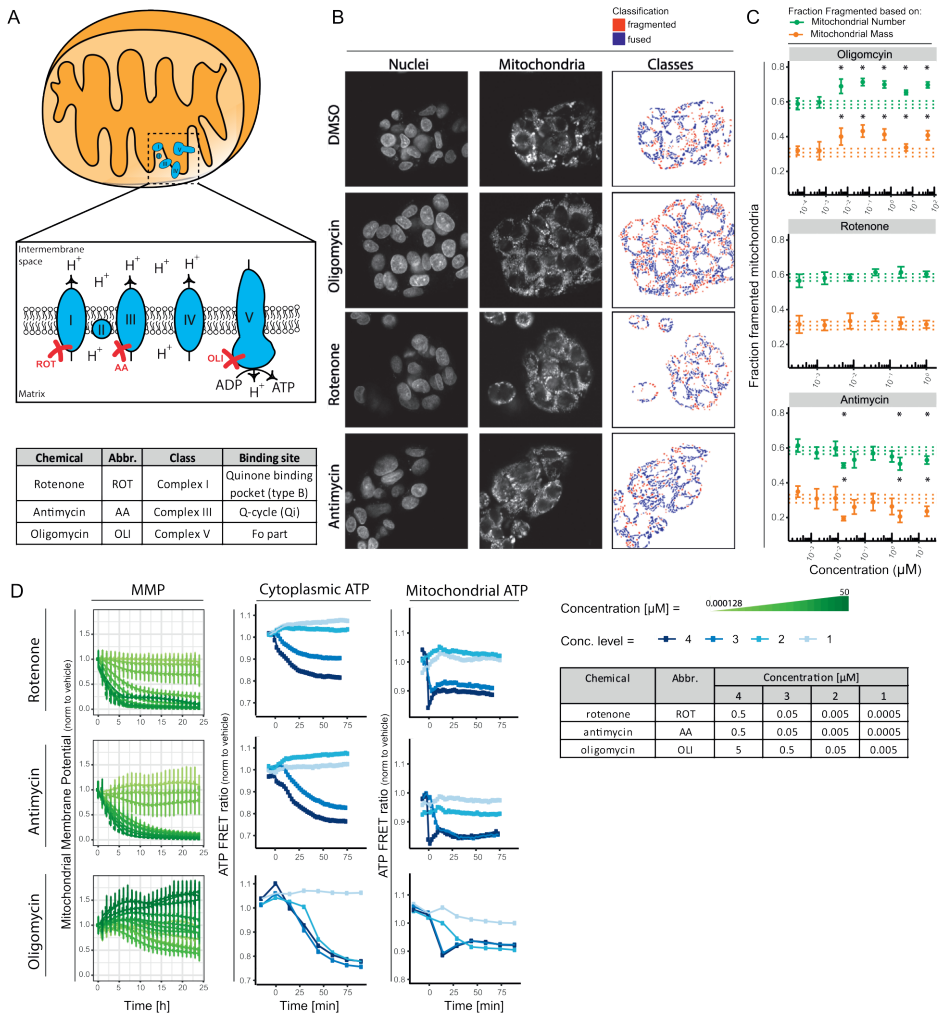


Figure 2: Quantitative analysis of ATP and MMP for 3 ETC complex inhibitors

A) Schematic representation of the ETC in mitochondria showing the different complexes involved, the creation of a proton gradient and the synthesis of ATP. Table includes information per compound concerning class and binding site. **B)** Representative confocal imaging pictures of HepG2 cells stained with Hoechst (nuclei) and MitoTracker Red (mitochondria) and exposed for 24h to vehicle control, 1µM rotenone, 1µM antimycin or 5µM oligomycin. The MitoTracker Red pictures were analyzed using the pipeline describe in Fig. 1, which resulted in a distribution into two populations (red = fragmented, blue = fused). **C)** Fraction of mitochondria belonging to the class of fragmented mitochondria following 24h exposure to vehicle control or a concentration range of oligomycin, rotenone or antimycin. The two colors represent two methods: based on the number of identified objects (green) or incorporation of the identified object mass (orange). Data is represented as mean plus SE of three biological replicates. The dotted lines represent the average and SE of the vehicle treatment (0.2 v/v% DMSO). Asterisk represent a p-value < 0.05 for the comparison to the vehicle control. **D)** Quantification of mitochondrial parameters upon exposure to a concentration range of rotenone, antimycin or oligomycin. From left to right: MMP over time after exposure to 10 concentrations ranging from 0.000128 to 50µM (data is represented as a mean of 4 biological replicates ±SD); cellular ATP levels over time upon exposure to 4 concentrations quantified using an ATP-biosensor (the presented data is from one replicate, additional biological replicates are shown in Suppl. fig 2); mitochondrial ATP levels over time upon exposure to 4 concentrations quantified using an ATP-biosensor (the presented data is from one replicate, additional biological replicates are shown in Suppl. fig 2). Table includes the concentrations selected for the ATP-FRET measurements.

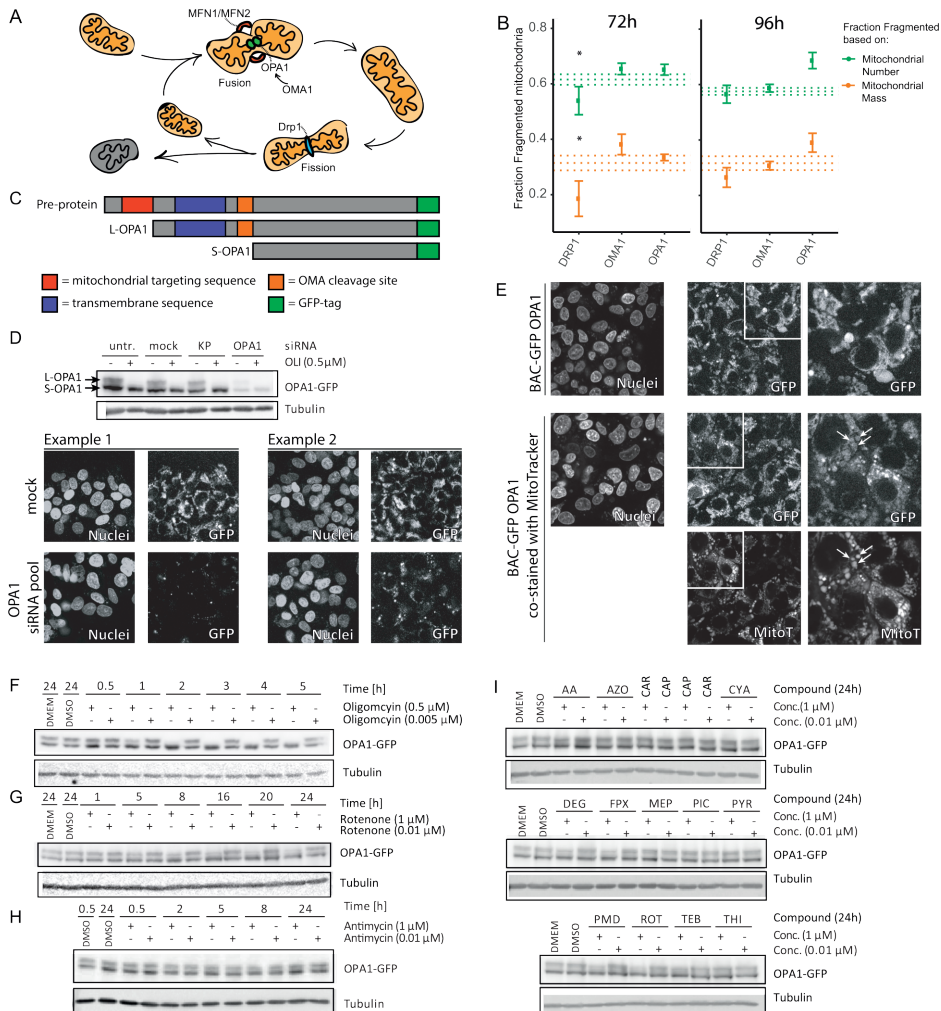


Figure 3: OPA1 cleavage correlates with mitochondrial fragmentation

A) Picture demonstrating the relationship between the process of fission and fusion and its major players. MFN1/ MFN2 together with the membrane bound form of OPA1 are involved in mitochondrial fusion. OMA1 de-activates OPA1 via cleavage. DRP1 together with the endoplasmic reticulum are responsible for mitochondrial fission. **B**) Fraction of mitochondria belonging to the class of fragmented mitochondria 72h or 96h after silencing of *DRP1*, *OMA1* and *OPA1*. The two colors represent two methods for determination of the fraction: based on the number of identified objects (green) or incorporation of the identified object mass (orange). Data is represented as mean plus SE of three or two biological replicates, respectively for 72h and 96h. The dotted lines represent the average and SE of the mock condition. Asterisk represent a p-value < 0.05 for the comparison to the vehicle control (no statistics were performed for the 96h samples). **C**) Scheme demonstrating the different forms of OPA1. **1**) the pre-protein including mitochondrial targeting sequence and transmembrane sequence. **2**) OPA1 is cleaved into L-OPA1 after entering the mitochondria. **3**) L-OPA1 can be cleaved into S-OPA1 by OMA1 resulting in the loss of the transmembrane domain. The creation of a OPA1-GFP fusion protein using BAC technology resulted in a C-terminally tagged protein. **D**) Western blot results for the BAC-GFP OPA1 cell line cultured in absence or presence of oligomycin (0.5μM) in combination with the indicated siRNAs (untr, untreated; mock, transfection reagent only; KP, kinase pool; OPA1, siRNAs targeting OPA1). Samples were stained with anti-GFP and anti-tubulin. Lower part: Representative confocal images of HepG2 BAC-GFP OPA1 cells treated with mock or siRNAs targeting OPA1. **E**) Representative confocal images of the HepG2 BAC-GFP OPA1 reporter cell line demonstrating the overlap of GFP signal and MitoTracker Red. **F**) Western blot results showing GFP and tubulin in HepG2 BAC-GFP OPA1 cells treated with 2 concentrations oligomycin (0.005 or 0.5μM) for 0.5, 1, 2, 3, 4, 5h. **G**) Western blot results showing GFP and tubulin in HepG2 BAC-GFP OPA1 cells treated with 2 concentrations rotenone (0.005 or 0.5μM) for 1, 5, 8, 16, 24h. **H**) Western blot results showing GFP and tubulin in HepG2 BAC-GFP OPA1 cells treated with 2 concentrations antimycin (0.005 or 0.5μM) for 0.5, 2, 5, 8, 24h. **I**) Western blot results showing GFP and tubulin in HepG2 BAC-GFP OPA1 cells treated with 2 concentrations (0.1 or 1μM) of 14 ETC complex inhibitors or controls for 24h.

To investigate how changes in the molecular machinery controlling fission/fusion related to the changes in morphology caused by ETC inhibition, we first focused on oligomycin. The increased fragmentation induced by this compound (Fig. 2B, C) was indeed accompanied by a proteolytic cleavage leading to a loss of the L-OPA variant at 2h (Fig. 3D, F; Suppl. fig 2B, C). We next analyzed post-translational modification of OPA1 in response to rotenone and antimycin that each induced a similar decrease in ATP in the cytoplasm and mitochondria as observed with oligomycin (Fig. 2D; Suppl. fig 1). Like oligomycin, rotenone exposure resulted in a reduction of L-OPA1, albeit less pronounced leaving a residual L-OPA1 expression perhaps explaining the lack of effect of rotenone on mitochondrial morphology (Fig. 3G; Fig. 2D; Suppl. fig 2D). By contrast, but in agreement with its effect on mitochondrial morphology, antimycin exposure failed to induce L-OPA1 cleavage, despite the loss of ATP triggered by this compound (Fig. 3H; Fig. 2D; Suppl. fig 2E). Together, these results indicated that mitochondrial fragmentation in response to ETC inhibition largely correlated with L-OPA1 cleavage, but activation of this process cannot be explained by ATP depletion alone.

Testing a larger panel of complex I and III inhibitors

We next compiled a larger set of chemicals all belonging to the classes of complex I and III inhibitors and supplemented this set with 3 complex II inhibitors. Previous work demonstrated that all complex I and III inhibitors, except for capsaicin and cyazofamid, but not complex II inhibitors, attenuated basal oxygen consumption rate (OCR), and specificity for the assigned complexes was confirmed [van der Stel 2020] (Suppl. fig 2F). A 24-hour exposure to concentrations above or around the OCR IC50 value for all active inhibitors did not result in a loss of L-OPA1. We only observed a minimal decrease of L-OPA1 upon exposure to complex I inhibitors pyrimidifen, rotenone and tebufenpyrad (Fig. 3I; Suppl. fig 2G). The absence of major reductions in L-OPA1 levels upon exposure to complex I and III inhibitors further indicated that a drop in ATP and OCR triggered by complex I and III inhibitors, by itself cannot explain OPA1 cleavage. Rather, the complex V inhibitor oligomycin, in addition to ATP and OCR inhibition, must connect to OPA1 cleavage and mitochondrial fragmentation in another manner.

Complex V inhibition also triggers OPA1 cleavage and mitochondrial fragmentation

While complex I, III, and V inhibition attenuated ATP levels and OCR, a distinguishing response to the complex V inhibitor oligomycin, as compared to the complex I and III inhibitors, was the increase in MMP in association with OPA1 cleavage and mitochondrial fragmentation. Two other chemicals known to inhibit complex V are DCCD and diafenthuron (DIA) (Fig. 4A) [Hong 2008, Krieger 2001]. As observed for active complex I and III inhibitors and the complex V inhibitor oligomycin, DCCD and DIA exposures resulted in an ATP decrease although the response was delayed

as compared to other compounds (Fig. 4B row 1 and 2; Suppl. fig 3A, B and C). Like oligomycin, DCCD and DIA triggered an increase in MMP, albeit at later time points as compared to oligomycin and only at lower concentrations (Fig. 4B row 1 and 2). Moreover, a 5h-exposure to 2 μ M DCCD also resulted in a loss of L-OPA1 and exposure to 2 μ M DIA resulted in a loss of L-OPA1 after 24h (Fig. 4C; Suppl. fig 3D). Finally, exposure to DCCD and DIA, similar to oligomycin, induced a concentration-dependent increase in the fraction of fragmented mitochondria (Fig. 4B row 1 and 2). These findings showed that the reduction in ATP levels and OCR combined with an increase in MMP that specifically characterized complex V inhibition, may trigger OPA1 cleavage and mitochondrial fragmentation.

Increase in MMP by itself is insufficient to trigger mitochondrial fragmentation

To assess if the increase in MMP per se was sufficient to trigger in mitochondrial fragmentation, we included Cyclosporin A (CSA), which affects the MMP via a non-ETC mechanism by blocking the mPTP pore resulting in a reduced exchange/leakage of protons between inner membrane space and mitochondrial matrix [Cassarino 1998, Waldmeier 2002, Mishra 2019]. Exposure to CSA resulted in an increased MMP without any effect upon ATP levels (Fig.4B row 3; Suppl. fig 3A, B and C). CSA treatment did not affect OPA1 cleavage (Fig. 4C; Suppl. fig 3D) and effects on mitochondrial morphology were observed only at the highest concentration tested (Fig. 4B row 3). Visual inspection of the mitochondrial morphology demonstrated that CSA caused a change in organelle structure but not a fragmentation such as observed with Oligomycin, DCCD or DIA exposure (Fig. 4D). These findings indicate that the increase in MMP, by itself is not sufficient to trigger OPA1 cleavage and mitochondrial fragmentation.

OPA1 depletion similarly triggers mitochondrial fragmentation but does not enhance toxicity of ETC inhibition

As our findings indicated selective OPA1 cleavage (causing a loss of OPA1 function) in the subset of ETC inhibitors triggering mitochondrial fragmentation, we tested the effect of OPA1 depletion by itself. Silencing *OPA1* resulted in an increase in fragmented mitochondrial objects that was similar to the level induced by Oligomycin (Fig. 5A; compare dashed line in right panel to blue curve in left panel). Combining OPA1 depletion with oligomycin treatment did not further increase mitochondrial fragmentation.

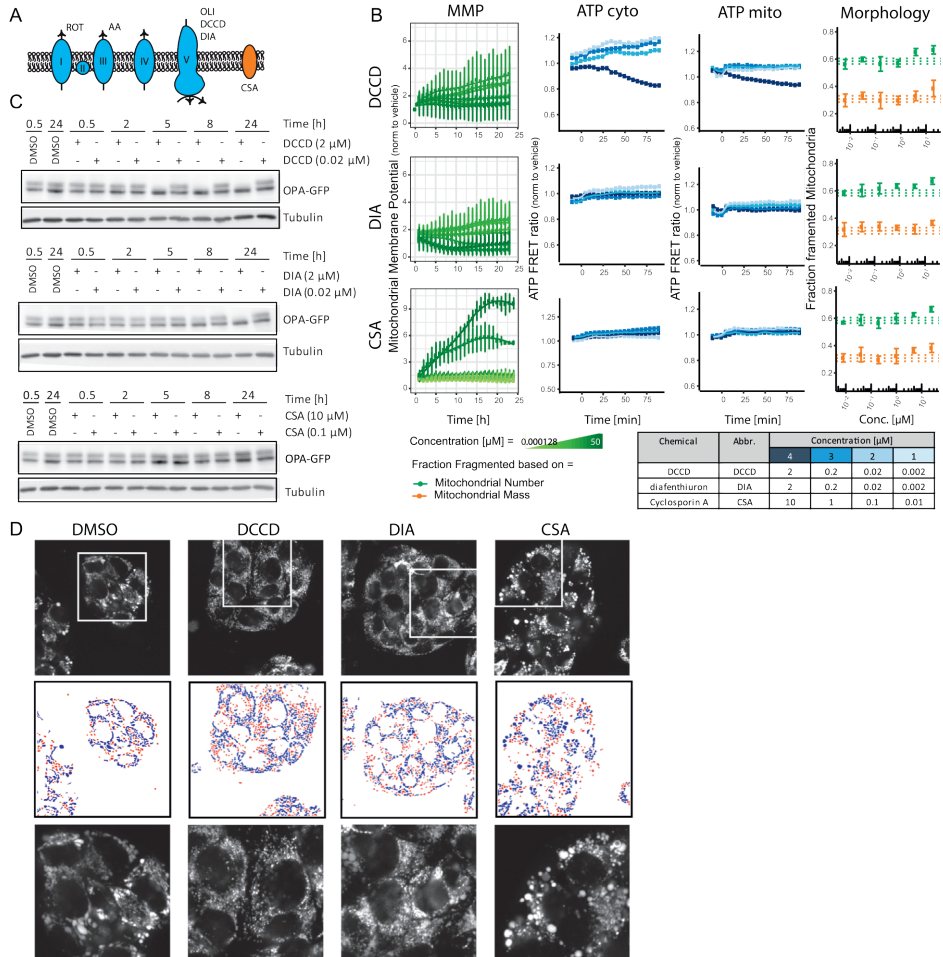


Figure 4: Impact of additional mitochondrial toxicants on mitochondrial function, morphology, and OPA1 cleavage

A) Schematic representation of the molecular target of the different mitochondrial inhibitors used in this study. **B)** Quantification of mitochondrial parameters after exposure to a concentration range of DCCD, DIA and CSA. The panels represent from left to right: mitochondrial membrane potential over time after exposure to 10 concentrations ranging from 0.000128 to 50 μM (data is represented as a mean of 4 biological replicates ±SD); cellular ATP levels over time after exposure to 4 concentrations quantified using cytoplasmic ATP-biosensor (presented data is from one replicate, additional biological replicates are shown in Suppl. fig 4); mitochondrial ATP levels over time after exposure to 4 concentrations quantified using mitochondrial-targeted ATP-biosensor (presented data is from one replicate, additional biological replicates are shown in Suppl. fig 4); fraction of mitochondria belonging to the class of fragmented mitochondria after chemical exposure. The two colors represent two methods: based on the number of identified objects (green) or incorporation of the identified object mass (orange). Data is represented as mean plus SE of three biological replicates. The dotted lines represent the average and SE of the DMSO condition. Asterisk represent a p-value < 0.05 for the comparison to the vehicle control. **C)** Western blot results showing GFP and tubulin in HepG2 BAC-GFP OPA1 cells treated with 2 concentrations DCCD (0.02 or 2 μM), DIA (0.02 or 2 μM) or CSA (0.1 or 10 μM) for 0.5, 2, 8, 24h. **D)** HepG2 cells stained with Hoechst and MitoTracker Red (mitochondria) and exposed 24h to vehicle control, 4 μM DCCD, 4 μM DIA or 25 μM CSA. Top row are representative high confocal imaging pictures. Middle row result of segmentation pipeline demonstrating the distribution into two populations (red = fragmented, blue = fused). Bottom row demonstrates a zoom-in from top panel.

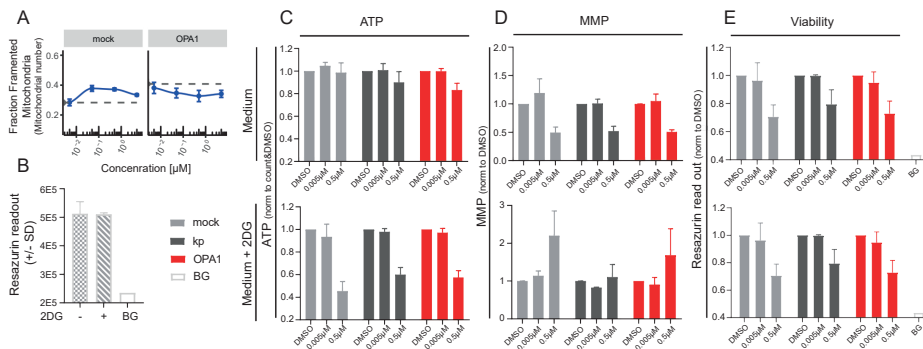


Figure 5: Effect of OPA1 silencing on mitochondrial morphology, viability, MMP and ATP

A) Fraction of mitochondria belonging to the class of fragmented mitochondria treated 72h with or without OPA1 siRNAs followed by 24h oligomycin (0.005, 0.05, 0.5 and 5 μ M) or vehicle (0.2 v/v% DMSO) exposure. Data is represented as mean fragmented fraction plus SE (based on number of objects identified) of three biological replicates. The dotted lines represent the average of the vehicle exposure. **B)** Quantification of viability based on resazurin conversion for medium with/without 2DG after 96h after KD. Data is representation of mean plus SD of 3 replicates (BG, background signal). **C-E)** Quantification of mitochondrial parameters in cells treated 72h with indicated siRNAs (see legend Fig. 5B) followed by exposure to oligomycin (0.005, 0.5 μ M) in medium with/without 2DG. Data is represented as a mean of 3 biological replicates plus SD) **C)** Total cellular ATP levels quantified using ATPlite assay after 5h oligomycin exposure. **D)** Mitochondrial membrane potential at 24h oligomycin exposure. **E)** Quantification of viability based on resazurin conversion after 24h oligomycin exposure.

We assessed whether OPA1 depletion by itself led to toxicity under regular cell culture conditions and in presence of 2-deoxyglucose (2DG) to enforce a strict dependence on mitochondrial respiration. 2DG was added to the medium at a level that did not affect cellular viability per se (Fig. 5B). OPA depletion did not affect ATP levels, MMP, or viability by itself under control or 2DG conditions (Fig. 5C-D). Moreover, the reduction in ATP, the increase in MMP, and the reduced viability observed with 0.5 μ M oligomycin was not amplified by OPA1 depletion.

Taken together, our findings identify a combination of reduced ATP levels and OCR and increased SE as the trigger for mitochondrial fragmentation that is observed with exposure to ETC complex V and a subset of complex I and III inhibitors. We find that this combination is intimately connected with OPA1 cleavage and OPA1 silencing is sufficient to trigger a similar mitochondrial fragmentation. This level of fragmentation cannot be assigned to a (mal)adaptive response as OPA1 silencing by itself does not affect viability and fails to (de)sensitize cells to ETC inhibition.

Discussion

In this work, we assessed the interconnectivity of mitochondrial morphology, MMP, and ATP production in the context of chemical exposure to distinct ETC inhibitors. Our results demonstrate that the different mitochondrial morphologies, fused or fragmented organelles, can be reliably quantified in a high throughput, confocal imaging setup. We identified that changes in ATP or MMP alone could not explain the observed chemical-induced changes in mitochondrial morphology. Our data indicates that the integration

of multiple mitochondrial features in a time- and concentration-dependent approach will improve mechanism-based characterization of mitochondrial toxicants.

Changes in mitochondrial morphology have been linked to alterations in MMP, production of ATP, and other mitochondrial processes [Anand 2014, Baker 2014, Ehses 2009, Head 2009, Consolato 2018]. We combined real time confocal microscopy analysis of mitochondrial morphology, MMP, and ATP levels to assess their temporal relationships in the context of exposure to concentration ranges of ETC complex inhibitors. We used a set of mitochondrial toxicants with a well-defined mode-of-action. The observed mitochondrial objects were quantified based on size and shape descriptors used in earlier studies: area, perimeter, formfactor and solidity [Bondi 2016, Irobi 2012, Rodríguez-Martin 2016]. The use of an unsupervised machine learning pipeline enabled us to separate fragmented and fused objects based on the measured object features. Other have reported a correlation of mitochondrial fission with the perimeter and solidity of the detected objects [Westrate 2014]. The larger variance observed in our data for the size descriptors (area and perimeter) compared to the shape features (solidity and formfactor) indicates that fragmented and fused mitochondria are more easily distinguished by their shape than by their size. Because of the used set of mitochondrial toxicants, the established model is biased towards identification of smaller objects and would benefit from a more diverse set of treatments including those enhancing fusion or inhibiting fission. As an alternative, supervised learning can be employed for mitochondrial classification purposes [Leonard 2015, Peng 2011]. However, supervised learning is based on example mitochondrial objects and requires high resolution images for identification of detailed object features. Our approach is applicable to lower resolution images and therefore fits more readily to high throughput approach. This creates the opportunity to systematically screen large sets of chemicals for their effects upon mitochondrial morphology.

This setup also allowed us to combine high throughput analysis of mitochondrial morphology with other, functional mitochondrial readouts developed for the same imaging format. For this purpose, we focused on MMP using dyes depending on MMP to accumulate in mitochondria and on the production of ATP using ATP biosensors localized in mitochondria or in the cytoplasm. A decrease in MMP [Jones 2017] or a decrease in ATP [Jones 2017] have been reported to drive OPA-mediated changes in morphology. Our findings show that the relationship between MMP, ATP production, and mitochondrial morphology is more complex and, unexpectedly, only ETC complex inhibitors causing an increase in MMP trigger OPA1 cleavage and mitochondrial fragmentation. Importantly, increasing MMP alone by blocking the mPTP pore does not lead to OPA1 cleavage and mitochondrial fragmentation. Instead, a combination of MMP increase with a reduction in ATP production and OCR is what characterizes

the ETC complex I, III, and V inhibitors that trigger mitochondrial fragmentation. Indeed, this subset of ETC complex inhibitors also trigger OPA1 cleavage. Moreover, OPA1 silencing is sufficient to trigger a similar mitochondrial fragmentation. These findings suggest a delicate control of the upstream regulators of OPA1 cleavage such as the protease OMA1, which acts as a sensor for mitochondrial stress [Baker 2014].

We find no evidence that mitochondrial fragmentation associated with OPA1 cleavage represents a (mal)adaptive response. First, OPA1 silencing, which causes a similar level of mitochondrial fragmentation as observed with the subset of ETC complex inhibitors, by itself does not affect ATP production or cell viability. Secondly, OPA1 silencing does not (de)sensitize cells to ETC inhibition. In other *in vitro* and *in vivo* systems, overexpression of OPA1 or another fusion related protein, MFN resulted in protection against mitochondria-related toxicities and disease [Hwang 2014, Alaimo 2014, Patten 2014, Civiletto 2015]. Vice versa, overexpression of the fission protein DRP1 worsened rotenone toxicity in *drosophila* [Hwang 2014] while pharmacological inhibition of Drp1 with mdivi protects cells against oxygen–glucose deprivation [Grohm 2012, Tian 2014]. The reason for the apparent discrepancy between these studies and our own finding is not clear but the modest shift from fusion to fission achieved by OPA1 silencing or by ETC complex inhibition in our study may be tolerated while strong overexpression, a full KO, or pharmacological inhibition of fusion/fission proteins may impact on viability.

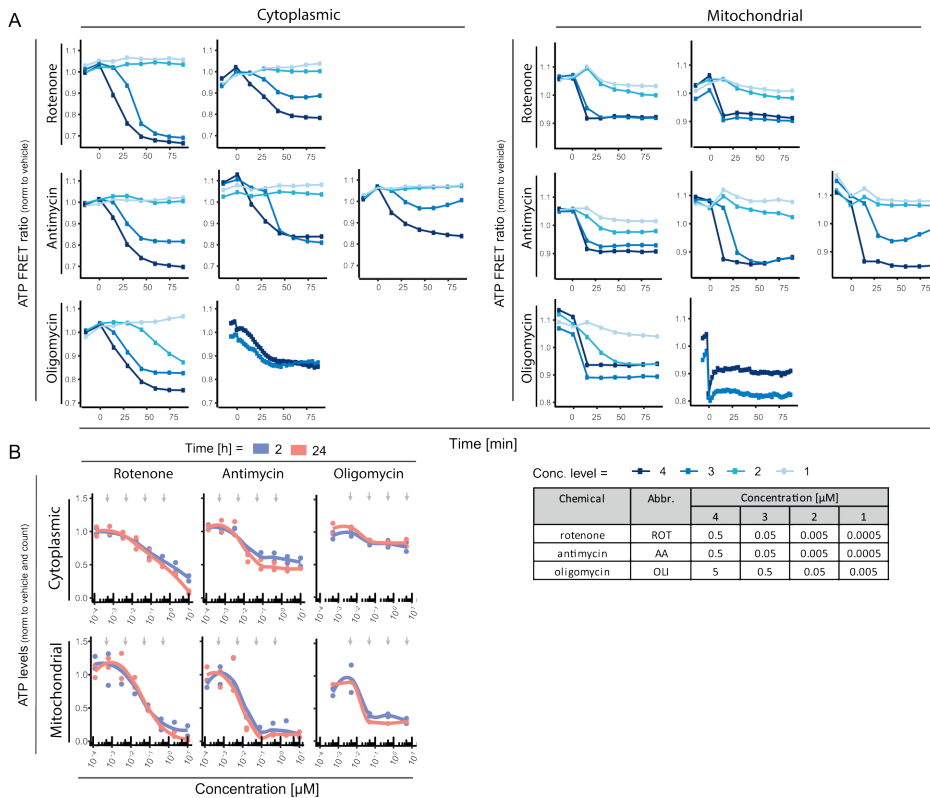
In addition to providing new insight in the relationship between different responses to ETC complex inhibition (mitochondrial morphology, MMP, cellular and mitochondrial ATP, cell viability) this study sets the stage for large scale chemical screening using multi-parameter microscopic readouts. The next generation chemical risk assessment paradigm stimulates the use of mechanism-driven studies in which biology-relevant parameters are quantified using sophisticated unbiased assessment methods and integrated into networks of prediction models [Krewski 2014]. The data obtained in this study fits this type of risk assessment, when combined with for instance ordinary differential equations (ODEs) to describe the time and concentration dependency of the ATP and MMP alterations [Yang 2021 submitted, Daun 2008]. Such modeling efforts will result in threshold values describing the concentration, moment in time or the effect size at which one event will trigger the next. This process will benefit from the incorporation of single cell measurements describing multiple events in one cell, which will enable establishment of relationships e.g. between ATP, MMP, and distribution of mitochondrial objects. The time- and concentration-resolved multi-parameter data such as generated in this study can be applied in screening of a wider range of chemicals and provide quantitative data for adverse outcome pathway (AOPs) [Leist 2017].

Acknowledgements

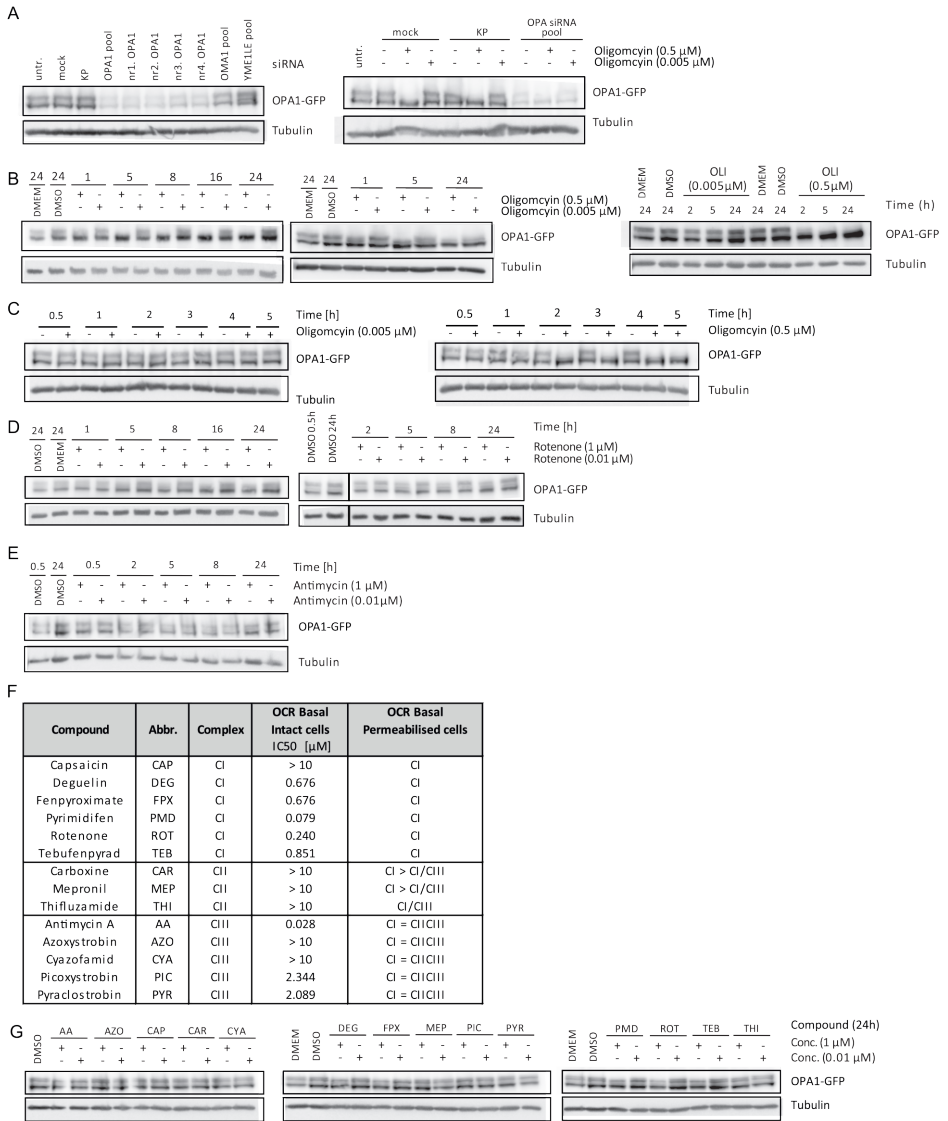
This project has received funding from the European Union's Horizon 2020 research and innovation programme under grant agreement No 681002.

We are grateful to Hans de Bont (Leiden University Cell Observatory) for his support & assistance in the morphology microscopy used in this work.

Supplementary material

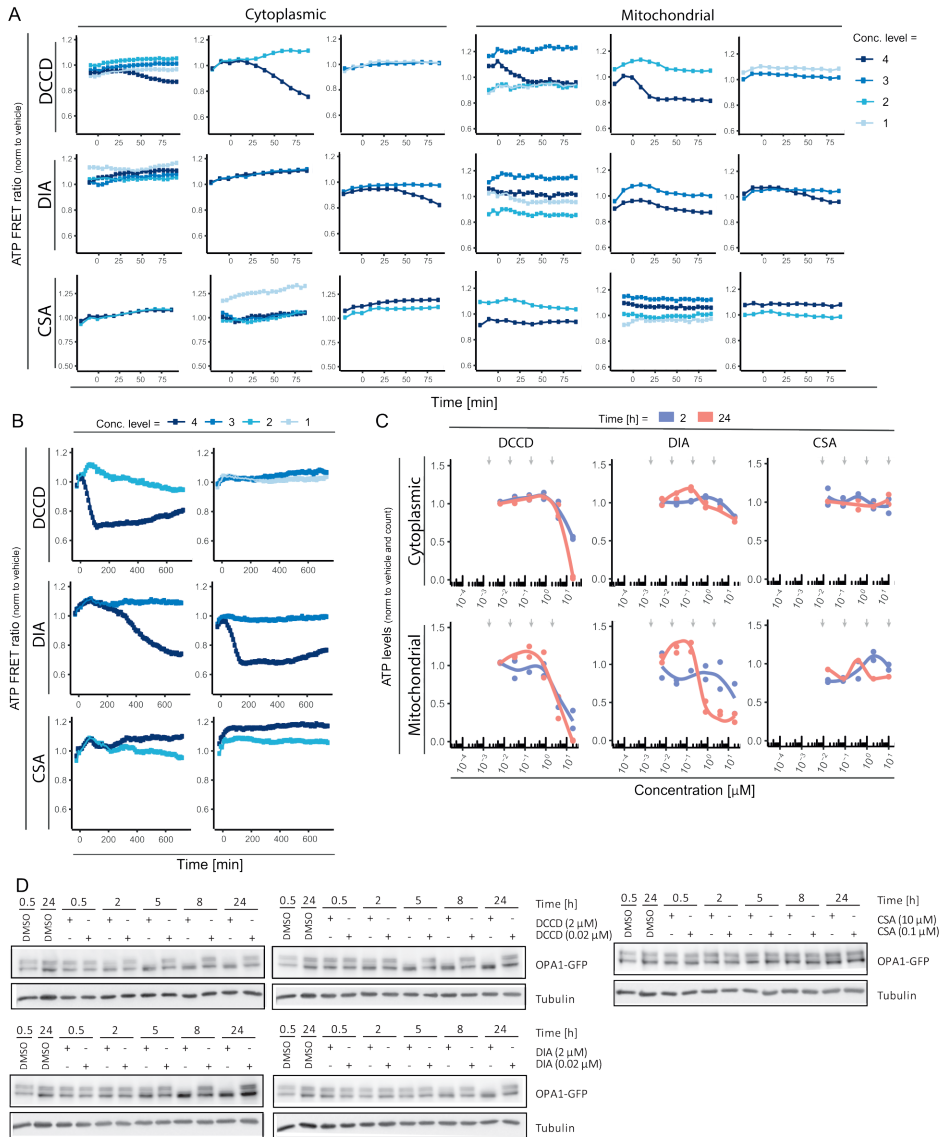
**Supplementary figure 1: Quantitative analysis of ATP and MMP for 3 ETC complex inhibitors**

Quantification of mitochondrial parameters after exposure to a concentration range of Rotenone, antimycin and oligomycin. **A)** Cellular and mitochondrial ATP levels over time upon exposure to 4 concentrations quantified using an ATP-biosensor. Individual biological replicates are shown. Table shows concentration 1-4 per compound. **B)** Total cellular and mitochondrial ATP levels measured using ATPlite assay at 2 and 24h exposure to a concentration range of the chemical. Data represents two biological replicates plus fit. Grey arrows represent the concentrations used in Fig2D and suppl. fig 2A.



Supplementary figure 2: OPA1-GFP cleavage in response to ETC complex inhibitors

A) Left: Western blot results of the BAC-GFP OPA1 cell line after OPA1 (pool and singles), OMA1 (pool) and YME1LE (pool) siRNA KD (untr, untreated; KP, kinase pool). Samples were stained with anti-GFP and anti-tubulin. Right: Western blot results of the BAC-GFP OPA1 cell line after OPA1 (pool) siRNA KD (untr, untreated; KP, kinase pool) combined with oligomycin treatment at 2 concentrations (0.005 or 0.5 μM). Samples were stained with anti-GFP and anti-tubulin. **B)** Western blot results showing GFP and tubulin in HepG2 BAC-GFP OPA1 cells treated with 2 concentrations oligomycin (0.005 or 0.5 μM) for 1, 2, 5, 8, 16, 24h. **C)** Western blot results showing GFP and tubulin in HepG2 BAC-GFP OPA1 cells treated with 2 concentrations oligomycin (0.005 or 0.5 μM) for 0.5, 1, 2, 3, 4, 5h. **D)** Western blot results showing GFP and tubulin in HepG2 BAC-GFP OPA1 cells treated with 2 concentrations rotenone (0.01 or 1 μM) for 1, 2, 5, 8, 16, 24h. **E)** Western blot results showing GFP and tubulin in HepG2 BAC-GFP OPA1 cells treated with 2 concentrations antimycin (0.01 or 1 μM) for 0.5, 1, 2, 5, 8, 24h. **F)** Table showing OCR results for intact and permeabilised cells (data generated in [van der Stel 2020]). **G)** Western blot results showing GFP and tubulin in HepG2 BAC-GFP OPA1 cells treated with 2 concentrations (0.1 or 1 μM) of 14 ETC complex inhibitors or controls for 24h.



Supplementary figure 3: Impact of additional mitochondrial toxicants on mitochondrial function, morphology, and OPA1 cleavage

A-C Quantification of mitochondrial parameters after exposure to a concentration range of DCCD, DIA and CSA. **A**) Cellular and mitochondrial ATP levels over time after exposure to 4 concentrations quantified using the ATP-biosensor (the presented data is from one 2 or 3 biological replicates). **B**) Cellular ATP levels over time (period of 12h) after exposure to 4 concentrations of DCCD, DIA or CSA quantified using cellular ATP-biosensor (the presented data is from one 2 or 3 biological replicates). **C**) Total cellular and mitochondrial ATP levels quantified using ATPlite assay at 2 and 24h exposure to a concentration range of the indicated chemicals. Data represents two biological replicates plus fit. Grey arrows represent the concentrations used in Fig. 4B, C and Suppl. fig 4A. **D**) Western blot results showing GFP and tubulin in HepG2 BAC-GFP OPA1 cells treated with 2 concentrations DCCD (0.02 or 2μM), DIA (0.02 or 2μM) and CSA (0.1 or 10μM) for 0.5, 2, 5, 8, 24h.

Supplementary information

Analysis Steps

For MitoTracker Red data:

- M1 obtain two dataframe files about metadata (Experimental information and Picture information),
- M2 run a python script to filter valid data (regarding the spatial resolution and quality of the images),
- M3 run a python script to find MitoTracker Red images (distinguish between nuclear (408nm) and mitochondrial (561nm) images) to segment mitochondria and get morphological features from segmented mitochondria,
- M4 run a python script to fitting a Gaussian mixture model based on all segmented mitochondria or subsampled part of all objects or objects from subsampled images.
- M5 run a python script to quantify response of mitochondria for each treatment based on image-level info, the response could be the fraction of count or mass of either fragmented or fused mitochondria, see details about the quantification in Appendix B.

For nucleus data:

- N1 generate a metadata file to instruct cellprofiler concerning the images to be analysed
- N2 run cellprofiler to segment the nuclei and store them as binary images,
- N3 run a python script to count the nuclei (also possible to count nuclei on the boundaries as fractional nuclei based on their size) or quantify the mass of nuclei

Quantification of classified mitochondria

Features concerning identified nuclei:

- count_nuclei_interior: number of nuclei who do not lie at boundaries
- count_nuclei_boundary: number of nuclei lying at boundaries
- totalMass_interiorNuclei: total mass of nuclei who do not lie at boundaries (based on mass of segmented objects).
- totalMass_boundaryNuclei: total mass of nuclei lying at boundaries (based on mass of segmented objects)
- count_nuclei_fractional: number of nuclei by counting the nuclei at boundaries as fractional nuclei (based on mass of segmented objects)

Features concerning identified mitochondria:

- nFragmentedMito: number of fragmented mito per image
- nFusedMito: number of fused mito per image
- nTMito: total number of mito per image

- aSumFragmentedMito: sum of mass of fragmented mito per image
- aSumFusedMito: sum of mass of fused mito per image
- fractionFragmentedMitoNumber: fraction of the count of fragmented mito
- fractionFragmentedMitoMass: fraction of the mass of fragmented mito

Features concerning both:

- nFragmentedMitoPerCell: number of fragmented mito per cell
- nFusedMitoPerCell: number of fused mito per cell
- nTMito: total number of mito per image
- aSumFragmentedMitoPerCell: sum of mass of fragmented mito per cell
- aSumFusedMitoPerCell: sum of mass of fragmented mito per cell
- nFragmentedMitoPerNucleiMass: number of fragmented mito normalized by total mass of nuclei
- nFusedPerNucleiMass: number of fused mito normalized by total mass of nuclei
- aSumFragmentedMitoPerNucleiMass: sum of mass of fragmented mito normalized by total mass of nuclei
- aSumFusedMitoPerNucleiMass: sum of mass of fused mito normalized by total mass of nuclei

